

# Competing Salt Effects on Phase Behavior of Protein Solutions: Tailoring of Protein Interaction by the Binding of Multivalent Ions and Charge Screening

Elena Jordan,<sup>#,†</sup> Felix Roosen-Runge,<sup>\*,#,†,‡</sup> Sara Leibfarth,<sup>†</sup> Fajun Zhang,<sup>\*,†</sup> Michael Sztucki,<sup>§</sup> Andreas Hildebrandt,<sup>||</sup> Oliver Kohlbacher,<sup>⊥</sup> and Frank Schreiber<sup>†</sup>

<sup>†</sup>Institut für Angewandte Physik, Universität Tübingen, Auf der Morgenstelle 10, 72076 Tübingen, Germany

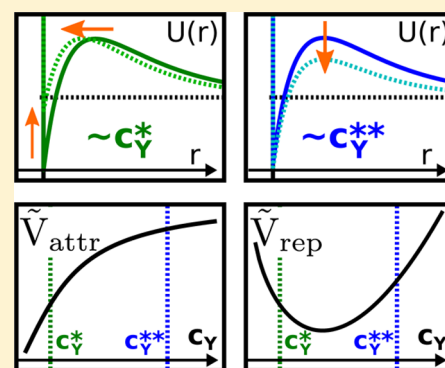
<sup>‡</sup>Institut Laue-Langevin, 71 Avenue des Martyrs, 38042 Grenoble, France

<sup>§</sup>European Synchrotron Radiation Facility, 71 Avenue des Martyrs, 38043 Grenoble, France

<sup>||</sup>Institut für Informatik, Universität Mainz, Staudingerweg 9, 55128 Mainz, Germany

<sup>⊥</sup>Zentrum für Bioinformatik, Zentrum für quantitative Biologie and Fachbereich Informatik, Universität Tübingen, Sand 14, 72076 Tübingen, Germany

**ABSTRACT:** The phase behavior of protein solutions is affected by additives such as crowder molecules or salts. In particular, upon addition of multivalent counterions, a reentrant condensation can occur; i.e., protein solutions are stable for low and high multivalent ion concentrations but aggregating at intermediate salt concentrations. The addition of monovalent ions shifts the phase boundaries to higher multivalent ion concentrations. This effect is found to be reflected in the protein interactions, as accessed via small-angle X-ray scattering. Two simulation schemes (a Monte Carlo sampling of the counterion binding configurations using the detailed protein structure and an analytical coarse-grained binding model) reproduce the shifts of the experimental phase boundaries. The results support a consistent picture of the protein interactions responsible for the phase behavior. The repulsive Coulomb interaction is varied by the binding of multivalent counterions and additionally screened by any increase of the ionic strength. The attractive interaction is induced by the binding of multivalent ions, most likely due to ion bridging between protein molecules. The overall picture of these competing interactions provides interesting insight into possible mechanisms for tailoring interactions in solutions via salt effects.



## INTRODUCTION

Salts are ubiquitous in nature. Under realistic physiological conditions, multiple types of salts are present and have profound effects on cellular processes. The interaction of salt ions with macromolecules such as proteins or DNA is a long-studied field with important open challenges. Starting with the Hofmeister series for ion-dependent effects of protein solubility,<sup>1–3</sup> the interaction of ions with aqueous surfaces shows interesting and manifold manifestations. The most basic one is the formation of the electrostatic double-layer as predicted by the Poisson–Boltzmann theory,<sup>4</sup> causing a screening of charges in electrolyte solutions. Ion condensation at the surface has been found for highly charged surfaces.<sup>5</sup> For multivalent salts, even a surface charge inversion due to condensed ions has been found to be caused by ion–ion correlations.<sup>6–10</sup> A similar charge inversion can also be observed in systems where ions bind to specific surface sites.<sup>11–15</sup> In the case of proteins, the coordinative binding of multivalent metal ions to functional groups on the protein surface has been studied intensively and found relevant under physiological conditions.<sup>16,17</sup>

For mixtures of mono- and multivalent salts, the picture of the ion–surface interaction becomes still more complicated. For the distributions of mono- and divalent counterions around DNA, competing effects between the two types of salts were found, at the same time supporting and challenging the applicability of the Poisson–Boltzmann theory for mixtures of ion types.<sup>4,18,19</sup> Regarding the effective charge inversion due to ion–ion correlations, theoretical approaches predict a so-called “giant overcharging”,<sup>20</sup> while simulations suggest that monovalent salt is lowering the effective reversed charge.<sup>21</sup> For the binding of multivalent ions to functional groups such as carboxylates in amino acids, the equilibrium constants are decreased slightly upon addition of monovalent salt.<sup>22</sup> In real systems such as protein solutions, these effects all occur simultaneously, rendering a complete description challenging.

A better description of the interaction between ions and macromolecules is important for the detailed understanding of macromolecular interactions and the related phase behavior.

Received: June 12, 2014

Revised: August 18, 2014

Published: September 2, 2014

For DNA, the ion condensation and a related reentrant condensation of DNA macromolecules have been studied intensively.<sup>19,23,24</sup> Reentrant condensation means that solutions are clear for low and high salt concentrations, indicating stable solutions. At intermediate multivalent salt concentration between the transition concentrations  $c^*$  and  $c^{**}$ , the solutions become turbid. It was found experimentally<sup>23</sup> as well as theoretically<sup>19,24</sup> that  $c^*$  increases with the addition of monovalent salt, suggesting that condensation of multivalent ions is weakened with increasing ionic strength.

In the context of phase behavior of biological solutions, proteins represent a challenging system. Controlling the phase behavior of protein solutions is a key goal in protein science. It has important implications for several biotechnological applications, for example, in protein crystallization or shelf life of biomedical products. Proteins have a nonspherical and rough shape with inhomogeneous patterns of surface charge and hydrophobicity. Thus, a variety of anisotropic forces can act between proteins, and theoretical results for model systems like spheres or rods can only be applied with care.

In this article, we study the role of monovalent (NaCl) and multivalent (YCl<sub>3</sub>) salts in solutions for the phase behavior of the globular protein human serum albumin (HSA). Recently it was found that multivalent ions induce a reentrant condensation in protein solutions.<sup>25–27</sup> This reentrant behavior can be understood by an inversion of the protein surface charge due to binding of Y<sup>3+</sup> ions to surface groups. This charge inversion has been found to be a universal behavior in protein solutions in the presence of multivalent metal counterions.<sup>26,27</sup> Both Monte Carlo sampling of the binding configurations<sup>25</sup> and an analytical coarse-grained model<sup>27</sup> reproduce the charge inversion with good qualitative and even reasonable quantitative agreement. Here we study the yet unexplored effect of monovalent salt on the charge inversion and reentrant phase behavior induced by multivalent salt to elucidate the underlying protein interactions.

## EXPERIMENTAL SECTION

**Materials.** Defatted human serum albumin (HSA) was purchased from Sigma-Aldrich (A 9511, essentially globulin-free). YCl<sub>3</sub> was purchased from Sigma-Aldrich as anhydrous powder with a high-purity grade (99.99%, no. 451363). NaCl (>99.5%) was purchased from Merck. Degassed Milli-Q water was used to prepare all solutions. All solutions were prepared and studied at room temperature (295 ± 2 K).

Stock solutions for the protein (HSA 200 mg/mL) and the salts (salt concentration 100 mM) were prepared and then diluted in order to obtain the desired concentrations. For SAXS measurements, the samples were centrifuged at 10 000 rpm for 5 min. The protein concentrations of the samples were determined by UV–visible spectroscopy using the absorption at 280 nm with an extinction coefficient for HSA of 0.531 L/(g cm). The pH of the solution was found to be close to 7 and did not vary significantly between different protein and salt concentrations. Note that this pH stability observed for the HSA/YCl<sub>3</sub>/NaCl system does not necessarily apply to other proteins and salts. Strong pH shifts are observed in systems where the metal ions undergo hydrolysis (e.g., FeCl<sub>3</sub>, AlCl<sub>3</sub>).<sup>27</sup> We remark that no dialysis or other purification of the samples was necessary, since the conclusions of the study are based on qualitative trends with increasing salt concentration, and the amount of counterions dissociating from the protein surface is expected to be lower than the concentration of monovalent salt.

**Protein Phase Diagram as a Function of Protein and Multivalent Salt Concentration.** In order to determine changes in the phase behavior qualitatively, the turbidity of the samples was determined by visual inspection 3–5 min after the preparation, when the opacity was constant. Simultaneously, the absorption was determined with UV–visible spectroscopy. Spectra were recorded in the wavelength range from 400–800 nm, where the protein shows no characteristic absorption. The transmitted intensity was integrated over the spectral range. The absorption increases significantly once the samples become turbid. The results from both methods are consistent.

In order to determine the transition concentrations, series of samples with the same protein concentration and various YCl<sub>3</sub> concentrations close to  $c_Y^*$  and  $c_Y^{**}$  were prepared. The highest YCl<sub>3</sub> concentration at which the sample is still clear,  $c_{Y1}$ , and the lowest YCl<sub>3</sub> concentration at which the sample is turbid,  $c_{Y2}$ , were determined. The first transition concentration  $c_Y^*$  with an inaccuracy of  $\delta c_Y^*$  was calculated as

$$c_Y^* = \frac{c_{Y1} + c_{Y2}}{2}, \quad \delta c_Y^* = \frac{c_{Y1} - c_{Y2}}{2} \quad (1)$$

$c_Y^{**}$  is determined analogously.

**Small-Angle X-ray Scattering (SAXS).** *Experiments.* SAXS measurements were performed at the European Synchrotron Radiation Facility (ESRF) in Grenoble, France, at the beamline ID02 with a sample-to-detector distance of 2 m. The energy of the incoming beam was 16.062 keV (wavelength 0.078 nm). A  $q$ -range from 0.072 to 4.5 nm<sup>-1</sup> was covered. The SAXS detector was a fiber-optically coupled fast-readout low-noise (FReLoN) CCD based on a Kodak KAF-4320 image sensor in an evacuated flight tube. About 100 μL of sample solution was filled into a flow-through quartz capillary. The sample in the scattering volume was exchanged for every exposure. For each sample, 10 exposures of 0.3 s each were measured. The 2D data were normalized to an absolute scale and azimuthally averaged to obtain the intensity profiles, and the solvent background was subtracted. More detailed information on data reduction and  $q$ -resolution calibration can be found in the literature.<sup>28</sup>

*Data Analysis.* Small-angle X-ray scattering data can be used to obtain information on the pair interaction potential.<sup>29–31</sup> The scattering intensity,  $I(q)$ , for a polydisperse or a nonspherical system can be calculated on the basis of approximation approaches such as the “decoupling approximation” and the “average structure factor” approximation.<sup>32,33</sup> Both approaches assume that the particle position is not correlated with its orientation. For the case of nonspherical but monodisperse solutes at a low to intermediate concentration, such as the studied protein solutions, both approaches give comparable results.<sup>34</sup> Therefore, in this work, the scattering intensity is calculated using the average structure factor approximation, which can be expressed by

$$I(q) = N(\Delta\rho)^2 V^2 P(q) \overline{S}(q) \quad (2)$$

where  $q = (4\pi/\lambda) \sin(2\Theta/2)$  is the scattering vector,  $2\Theta$  is the scattering angle,  $N$  is the number of protein molecules per unit volume in the solution,  $\Delta\rho = \rho_p - \rho_s$  is the scattering length density difference between the solvent and the solute, and  $V$  is the volume of a single protein.  $P(q)$  is the form factor of a given protein, i.e., the scattering from a single protein molecule after orientation averaging. An ellipsoid form factor with semiaxes  $a$  and  $b$  is used to model HSA:<sup>35</sup>

$$P(q) = \int_0^1 dx \left| \frac{3(\sin u - u \cos u)}{u^3} \right|^2 \quad (3)$$

$$u = qb[(a/b)^2 x^2 + (1-x)^2]^{1/2} \quad (4)$$

By use of the average structure factor approximation,  $\bar{S}(q)$  is calculated from a monodisperse structure factor with an effective sphere diameter. In the following parts and for simplicity, we use  $S(q)$  to denote  $\bar{S}(q)$ . In our case, the protein solution is a monodisperse but nonspherical (ellipsoidal) system. The effective sphere diameter  $\sigma$  is calculated by equating the second virial coefficient of the effective sphere and the ellipsoid with the ellipsoidal half-axes  $a$  and  $b$ .<sup>36,37</sup>

In solutions with monovalent salt and at smaller salt concentrations, the interparticle potential can be modeled reasonably well by the repulsive part of a full DLVO potential, i.e., a screened Coulomb potential:<sup>38,39</sup>

$$U_{\text{SC}}(r) = \frac{Z^2 e^2 \exp(\kappa\sigma) \exp(-\kappa r)}{\varepsilon(1 + \kappa\sigma/2)^2 r} \quad (\text{for } r > \sigma) \quad (5)$$

$\varepsilon$  is the dielectric constant of the continuous medium.  $r$  is the center-to-center distance between two particles with diameter  $\sigma$  and charge  $Q = Ze$ .

The inverse Debye screening length  $\kappa$  depends on the ionic strength  $I$ ,

$$\kappa = \sqrt{\frac{\varepsilon k_{\text{B}} T}{2N_{\text{A}} e^2 I}} \quad \text{and} \quad I = \frac{1}{2} \sum_{\alpha} n_{\alpha} Q_{\alpha}^2 \quad (6)$$

where  $n_{\alpha}$  and  $Q_{\alpha}$  denote the number density and charge of the ions of species  $\alpha$  (both monovalent and multivalent) in the solution. Note that while Debye–Hückel theory is expected to fail for solutions of multivalent ions, we use  $\kappa$  only to describe the free ions in solution, while condensed and bound ions are accounted for explicitly. Because of the low multivalent ion concentration, this assumption allows at least comparisons of qualitative trends with salt concentration.

A solution for the structure factor using the rescaled mean-spherical approximation (RMSA)<sup>40,41</sup> was used for the fits.<sup>42</sup>

## THEORETICAL MODELING

**Detailed Protein Structure: Monte Carlo Sampling of Ion-Binding Configurations.** By use of a high-resolution structure of human serum albumin (HSA) from the Protein Data Bank (code 1NSU),<sup>43</sup> the binding probabilities of multivalent ions to solvent-exposed carboxylate groups were calculated with a Monte Carlo approach. Results and further description of this method have been published previously.<sup>25,26</sup> In brief, an established approach for the calculation of protonation states of proteins<sup>44</sup> has been modified for the case of the binding of multivalent metal ions ( $Y^{3+}$ ). The protonation state of an individual protein was predicted with the H++ Web server.<sup>45</sup> All solvent-exposed carboxylic groups were regarded as potential binding sites for  $Y^{3+}$ . The intrinsic association constant for  $Y^{3+}$  at a carboxylic group was estimated from experimental values.<sup>22</sup> The site-specific association constants were calculated from the intrinsic constant corrected for effects of solvation using the thermodynamic cycle<sup>44</sup> for the association of  $Y^{3+}$  at a carboxylic group as model component. The electrostatic partition function of  $Y^{3+}$  binding to a single protein molecule was sampled in a Monte Carlo scheme<sup>25</sup> to determine the  $Y^{3+}$  binding probabilities as a function of the  $Y^{3+}$

concentration. Note that in this context the bound  $Y^{3+}$  ions can be treated explicitly at atomic resolution, which allows for explicit incorporation of strong ion correlations. As a consequence, the simulation approach can use classical Poisson–Boltzmann theory to predict the electrostatic potential at the  $Y^{3+}$  binding sites in the presence of water. All parameters involved in the simulation were taken from literature values.<sup>22,25,43</sup> Note that the Monte Carlo sampling includes the full ion–ion correlation between bound  $Y^{3+}$  ions and accounts for the full atomic detail of HSA. These effects are expected to dominate the less important ion–ion correlations in the bulk solution, which are not accounted for in the Poisson–Boltzmann approach.

The average number of the bound  $Y^{3+}$  ions was determined at several  $Y^{3+}$  concentrations. The net charge of the protein is calculated for different fixed concentrations of monovalent salt from the bare charge of the protein and the  $Y^{3+}$  ions bound to the protein. The  $Y^{3+}$  concentration used in this approach corresponds to the concentration in the surrounding bulk solvent and thus describes only the free  $Y^{3+}$  ions. In order to obtain the full  $Y^{3+}$  concentration in solutions with many protein molecules, both free ions and bound ions are added up:

$$c_{\text{Y}} = c_{\text{Y,free}} + n_{\text{Y,bound}} c_{\text{HSA}} / M_{\text{HSA}} \quad (7)$$

$n_{\text{Y,bound}}$  is the average number of  $Y^{3+}$  ions bound to one protein,  $c_{\text{HSA}}$  is the protein concentration in mg/mL, and  $M_{\text{HSA}} = 66\,500$  Da is the molecular weight of HSA.

The addition of monovalent salt (NaCl) is included by a change of the Debye screening length used in the Poisson–Boltzmann calculations as well as a small shift of the equilibrium constant for the binding of multivalent ions to carboxylate groups.<sup>22</sup> The full simulation setup has been repeated for each monovalent salt concentration, respectively.

**Coarse-Grained Model: Analytical Calculation Scheme for Protein Total Charge.** An analytical model for the binding of multivalent ions to a spherical particle, taking into account charge regulation of surface groups, counterion binding as well as pH effects due to hydrolysis of multivalent metal ions, has been developed recently.<sup>27</sup> The scheme is based on association reactions between the present ions and surface sites, the binding to which is further dependent on the total particle charge. A detailed description of the method as well as the choice of suitable model parameters solely based on literature values and theoretical estimates can be found in ref 27.

In this coarse-grained model, the addition of monovalent salt varies the surface potential via the Debye screening length  $\kappa$  and thus changes the binding equilibria of multivalent ions. The analytical scheme allows an investigation of the effects of monovalent ions on the binding of multivalent ions and the protein total charge at low computational cost.

**Estimation of Phase Boundaries in the Reentrant Phase Diagram.** Two methods have been used to estimate the transition  $Y^{3+}$  concentrations,  $c_{\text{Y}}^*$  and  $c_{\text{Y}}^{**}$ , from the calculated protein total charges and the related full DLVO potential.

**Charge Estimation.** The transition concentrations can be estimated directly under the assumption that the transition salt concentrations,  $c_{\text{Y}}^*$  and  $c_{\text{Y}}^{**}$ , correspond to transition protein charges  $Q^*$  and  $Q^{**}$ . Ignoring charge regulation of the protein and using the HSA charge without  $YCl_3$  of  $Q_0 \approx -11e$ , the transition charges can be related to specific numbers of bound  $Y^{3+}$  ions  $N \approx (Q^* - Q_0)/3$ . We chose  $Q^* = -5e$  and  $Q^{**} = 5e$ , corresponding to roughly two and five bound ions. Note that the exact choice of  $Q^*$  and  $Q^{**}$  does not change the obtained

trends, since the charge profile is a monotonic function in  $c_Y$  and  $c_{\text{NaCl}}$ .

**Barrier Estimation.** The full DLVO potential between two spherical particles with diameter  $\sigma$  is given by a screened Coulomb repulsion and a van der Waals term:<sup>38,46</sup>

$$U_{\text{DLVO}}(r) = U_{\text{SC}}(r) + U_{\text{vdW}}(r) \quad (8)$$

$$U_{\text{vdW}}(r) = -\frac{A}{12} \left( \frac{\sigma^2}{r^2 - \sigma^2} + \frac{\sigma^2}{r^2} + 2 \log \frac{r^2 - \sigma^2}{r^2} \right)$$

where  $A$  is the system-dependent Hamaker constant. At low ionic strength and large charges, the DLVO potential shows a maximum  $U_{\text{DLVO}}(r_{\text{max}})$ , representing a repulsive barrier.  $U_{\text{DLVO}}(r_{\text{max}})$  can be used to estimate the propensity for aggregation. In our case, we used  $A = 3k_B T$  and  $\sigma = 6.6$  nm as employed for a similar protein (bovine serum albumin) with realistic results.<sup>27,39</sup> As the criterion for the transition concentrations, we used  $U_{\text{DLVO}}(r_{\text{max}}) - U_{\text{DLVO}}(r_{\text{eq}}) = 1k_B T$ , where  $r_{\text{eq}} = (\sqrt{2/n})^{1/3}$  where the number density  $n$  is the maximized distance between the particles in the solution.<sup>27,47</sup> We remark that in our case  $U_{\text{vdW}}(r)$  represents an effective interaction arising from a potentially different physical mechanism of interaction as discussed later.

## RESULTS AND DISCUSSION

**Experimental Phase Diagram: Reentrant Condensation.** Experimental phase diagrams for HSA in the presence of both monovalent and multivalent ions were determined as described in the methods section. Several HSA concentrations  $c_{\text{HSA}}$  between 5–50 mg/mL and NaCl concentrations  $c_{\text{NaCl}}$  between 0–100 mM were chosen to determine the transition concentration  $c_Y^*$  between the clear regime I and the turbid regime II and the second transition concentration  $c_Y^{**}$  between regime II and the clear reentrant regime III. Figure 1 shows an example of a phase diagram for HSA with  $\text{YCl}_3$  and a constant NaCl concentration of 20 mM. In the phase diagram the added  $\text{YCl}_3$  concentration is plotted against the protein concentration in the sample. For  $\text{YCl}_3$  concentrations lower than  $c_Y^*$  and higher than  $c_Y^{**}$  the samples are clear (solution regime I and

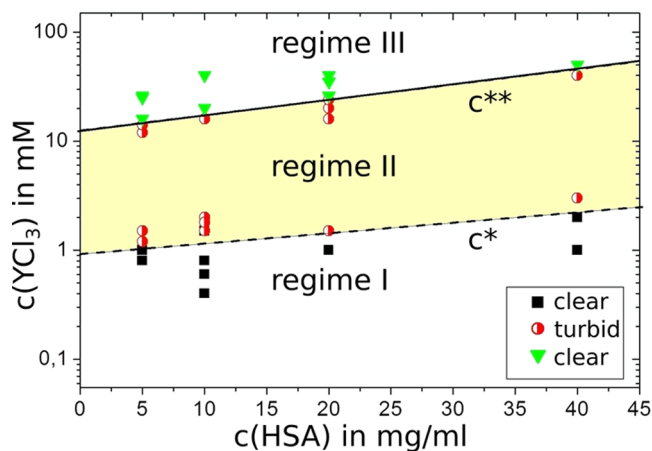


**Figure 1.** Phase diagram as determined by visual inspection for HSA with  $\text{YCl}_3$  and a constant NaCl concentration of 20 mM. Black squares stand for samples in the solution regime I, red circles for samples in the aggregation regime II, and green triangles for samples in the reentrant regime III. Samples in regimes I and III are clear, whereas samples in regime II are turbid because of aggregation.

reentrant regime III). Samples with  $\text{YCl}_3$  concentrations between  $c_Y^*$  and  $c_Y^{**}$  are turbid (aggregation regime II). Similar diagrams were generated for several different NaCl concentrations. Both transition concentrations  $c_Y^*$  and  $c_Y^{**}$  are found to increase with increasing  $c_{\text{NaCl}}$  as depicted in Figure 5a. This finding is discussed in more detail later together with simulation results.

The results from optical observation are also supported by measurements on the amount of precipitates. A set of samples was prepared with the same protein concentration of about 45 mg/mL, NaCl concentrations of 0.0, 10, 20, 50, and 80 mM, and various  $\text{YCl}_3$  concentrations between 2 and 40 mM. Aggregates formed after the addition of  $\text{YCl}_3$ , as predicted by the phase diagram. We centrifuged the samples to accelerate the precipitation. The protein concentration of the supernatant was monitored after centrifugation by UV–vis absorption. The results for 10, 50, and 80 mM NaCl are shown in Figure 2, indicating that the amount of precipitation also follows the reentrant behavior.

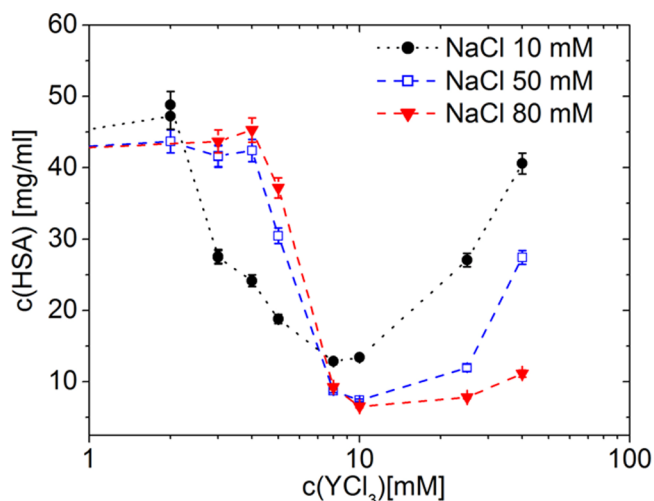


**Figure 2.** Protein concentration in the supernatant after the precipitation induced by  $\text{YCl}_3$ . The different colors refer to different NaCl concentrations (10, 50, 80 mM). With increasing NaCl concentration, both the initial aggregation and the redissolution occur at higher  $\text{YCl}_3$  concentrations.

The increasing trend of the transition concentrations  $c_Y^*$  and  $c_Y^{**}$  with increasing  $c_{\text{NaCl}}$  is recovered. At higher NaCl concentrations, higher  $\text{YCl}_3$  concentrations are required to cause precipitation. A similar trend is observed for the second transition, although no complete redissolution is obtained within the  $\text{YCl}_3$  concentration range between  $c_{\text{NaCl}} = 50$  mM and  $c_{\text{NaCl}} = 80$  mM.

For samples with  $c_{\text{HSA}} \gtrsim 30$  mg/mL with  $\text{YCl}_3$  and without NaCl, a liquid–liquid phase separation (LLPS) is found in regime II.<sup>48</sup> The investigation of NaCl effects on the LLPS was beyond the scope of this study, but we speculate that the underlying protein interaction causes qualitatively similar effects and trends.

**Variations of Protein Interaction throughout the Reentrant Condensation: SAXS.** SAXS data provide direct access to the protein interaction via liquid state theory fitting methods. Samples containing only NaCl and no  $\text{YCl}_3$  can be fitted very well with a form factor of an oblate ellipsoid with fixed semiaxes ( $a = 1.6$  nm and  $b = 4.2$  nm) and a screened

Coulomb structure factor. The results for a sample series with fixed HSA concentration  $c_{\text{HSA}} = 62 \text{ mg/mL}$ , no  $\text{YCl}_3$ , and increasing NaCl concentration ( $10 \text{ mM} < c_{\text{NaCl}} < 200 \text{ mM}$ ) are summarized in Figure 3a. For low NaCl concentrations, a pronounced correlation peak is observed, the height of which decreases with increasing NaCl concentration. This behavior can be explained by the screening of the protein charge and the reduction of the repulsive electrostatic interaction. The fit parameters at low salt concentration take realistic values (Table

1). With increasing NaCl concentration, the fitted volume fraction  $\varphi^{(\text{fit})}$  shifts to higher values, probably because the

**Table 1.** Fit Parameters for the Curves in Figure 3a<sup>a</sup>

$c_{\text{NaCl}}$ [mM]	$\varphi^{(\text{fit})}$ [%]	$Q^{(\text{fit})}$ [e]	$c_{\text{NaCl}}^{(\text{fit})}$ [mM]
10	6.6	-10.9	16
20	7.6	-10.5	21
50	7.8	-14.4	51
80	7.5	-14.1	81
200	8.1	-10.5	200

<sup>a</sup>The intensity from HSA, 62 mg/mL in NaCl solutions, is fitted with a screened Coulomb structure factor. The free fit parameters are shown in the table; the others were fixed. The parameters kept fixed were the semiaxes  $a = 1.6 \text{ nm}$  and  $b = 4.6 \text{ nm}$  of the oblate ellipsoid and the temperature  $T = 295 \text{ K}$ . The fit parameter for the salt concentration  $c_s(\text{NaCl})$  was first held on the prepared value and then let free for a second fit. The relative errors of the parameters were less than 1%.

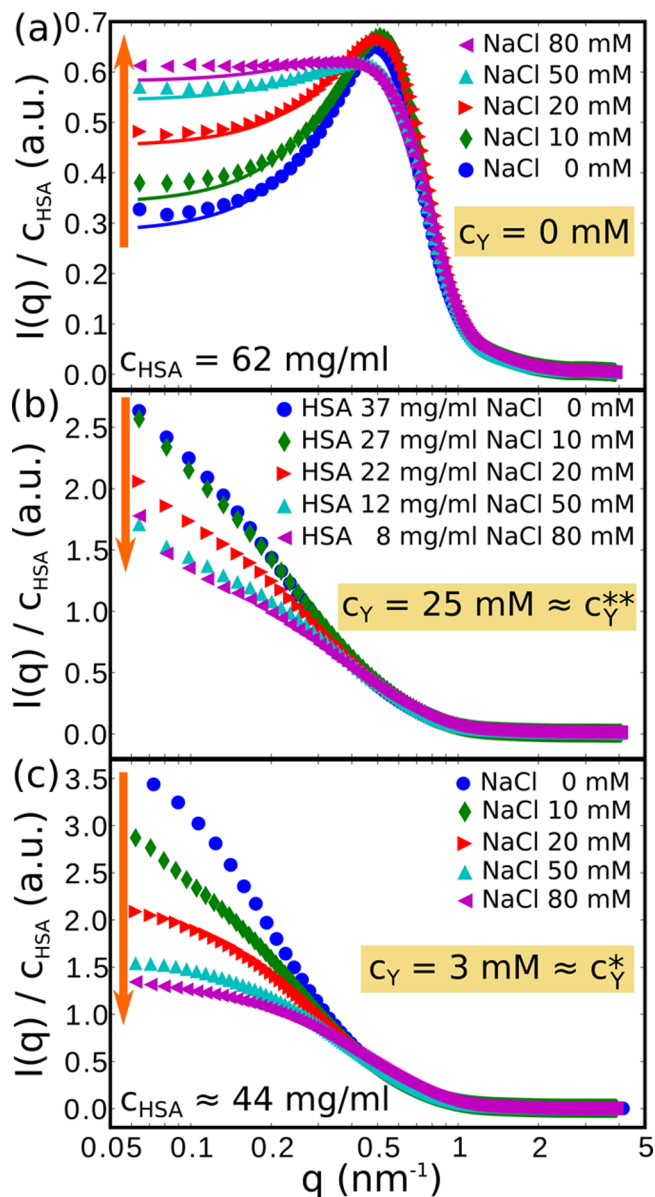


**Figure 3.** SAXS curves for HSA with different salt conditions. The orange arrows indicates the trend for increasing  $c_{\text{NaCl}}$ . For clarity, only every second data point is shown. (a) No  $\text{YCl}_3$ : With increasing  $c_{\text{NaCl}}$  the low- $q$  intensity increases due to the reduced screened Coulomb repulsion. The intensity is fitted using an ellipsoid form factor and a screened Coulomb structure factor (fit parameters, Table 1). (b)  $c_Y = 25 \text{ mM} \approx c_Y^*$ : The protein concentration in the measured supernatant decreases strongly with increasing  $c_{\text{NaCl}}$ , reflecting the increase of  $c_Y^*$  with  $c_{\text{NaCl}}$ . The scattering intensity in the limit of low  $q$  does not level off but increases steeply, thereby indicating the presence of larger aggregates. (c)  $c_Y = 3 \text{ mM} \approx c_Y^*$ : The low- $q$  intensity decreases with increasing  $c_{\text{NaCl}}$ , corresponding to weaker attractive interaction.

screened Coulomb structure factor becomes less accurate. The general results are consistent with results on protein interactions in charge-screened solutions of bovine serum albumin (BSA) at low to high protein concentrations<sup>34,47</sup> and results on HSA in water and buffer.<sup>49</sup>

Upon addition of  $\text{YCl}_3$ , the phase behavior changes qualitatively (cf. Figure 1). In order to monitor the protein interactions throughout the phase diagram and their dependence on NaCl concentration, SAXS intensities were recorded for HSA concentrations  $c_{\text{HSA}}$  between 5 and 50 mg/mL at  $\text{YCl}_3$  concentrations  $c_Y$  of 1–50 mM and with NaCl concentrations  $c_{\text{NaCl}}$  of 0, 10, 20, 50, and 80 mM. Protein interactions deep in the solution regime I, i.e., at low  $c_Y$ , can still be modeled reasonably well with a repulsive screened Coulomb interaction. In solutions close to the aggregation regime II or in the reentrant regime III, the protein interactions cannot be described by a repulsive interaction anymore, indicating the increasing relevance of attractive interactions. In the context of this study, we are interested in the changes of attraction and repulsion. Since information on this overall interaction can be obtained by model-free means from the low- $q$  intensity, no detailed data fitting is required.

In Figure 3c, a series with fixed HSA concentration  $c_{\text{HSA}} \approx 44 \text{ mg/mL}$  and fixed  $\text{YCl}_3$  concentration  $c_Y = 3 \text{ mM}$  is shown, corresponding to conditions close to  $c_Y^*$ . Around  $c_Y^*$  the effect of NaCl is most pronounced, since the overall interaction is expected to change from a charge-screened repulsion to attraction. The low- $q$  intensity increases for decreasing  $c_{\text{NaCl}}$ , indicating an increasing strength of the overall attraction. Note that the opposite behavior would be expected if only charge screening was relevant, since the screening reduces the repulsion and thus increases the overall attraction with increasing  $c_{\text{NaCl}}$ .

Figure 3b depicts HSA solutions at fixed  $c_Y = 25 \text{ mM}$ , corresponding to conditions around  $c_Y^*$ . The solutions were prepared at a HSA concentration  $c_{\text{HSA}} \approx 44 \text{ mg/mL}$  for a series of NaCl concentrations  $c_{\text{NaCl}}$ . Before measurement, the samples were centrifuged to remove large aggregates. With increasing  $c_{\text{NaCl}}$  the amount of precipitated aggregates increases strongly, reflecting the trend of increasing  $c_Y^*$  and leaving a smaller protein concentration in the measured supernatant. The scattering intensity around  $c_Y^*$  does not level off on the given  $q$  range, suggesting that larger aggregates are still present in the supernatant or forming again. The decreasing scattering

intensity with increasing  $c_{\text{NaCl}}$  is thus related to the internal structure of larger aggregates and no good indicator for varying protein interactions. The results will be exploited and discussed in more detail in the discussion section.

**Protein Charge Inversion as a Function of Ionic Strength.** Measurements of the electrophoretic mobility as well as simulations show an inversion of the protein net charge upon addition of multivalent metal ions.<sup>25–27</sup> The results from both simulation schemes (the Monte Carlo sampling of binding configurations and the analytical coarse-grained model) for the protein net charge  $Q$  as a function of the  $Y^{3+}$  concentration are shown in Figure 4. All charge curves show an inversion from

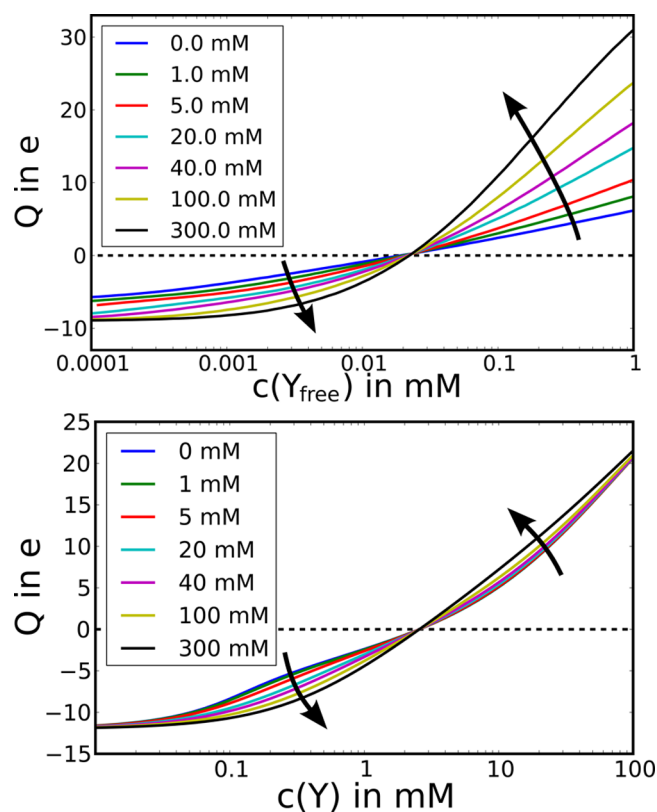


**Figure 4.** Charges of the protein–ion complex as a function of  $Y^{3+}$  concentration and for increasing NaCl concentration. Top: Net charges from Monte Carlo sampling of binding configurations. Bottom: Net charges from analytical coarse-grained model for a protein concentration of 5 mg/mL. The black arrows indicate the trends for increasing monovalent salt concentration. Note that the MC sampling method (top) is based on a single protein molecule; thus, no absolute protein concentration is provided and the salt concentration  $c_{Y,\text{free}}$  corresponds to the concentration of free ions in the solvent. The coarse-grained method uses a real salt concentration  $c_Y$  incorporating free and bound ions.

negative to positive net charge in the simulated range of  $Y^{3+}$  concentration, which is in qualitative agreement with experiments. Moreover, the simulated curves all meet at one point close to zero net charge for both approaches, respectively. This simple behavior suggests a dominant effect of the monopole moment on the cation binding compared to higher multipoles of the surface charges.

Both simulation schemes show similar trends with increasing monovalent salt concentration. In the regime of negative net charge a higher NaCl concentration leads to a lower number of bound  $Y^{3+}$  ions. This binding behavior is reasonable because

the favorable electrostatic interaction between the  $Y^{3+}$  ions and the negatively charged protein is weakened by the screening effect of the salt. In the regime of positive net charge the number of bound  $Y^{3+}$  ions increases with increasing NaCl concentration, since the electrostatic surface potential due to the positive protein net charge is decreased and thus allows more  $Y^{3+}$  ions to bind to the surface.

The differences between the simulations can be explained by the different nature of the underlying models. The differing  $Q$  spread at low salt concentration might be due to the fact that the coarse-grained model takes into account only one effective binding site, while the Monte Carlo scheme calculates the binding equilibrium for each site individually and, thus, incorporates a broader distribution of equilibrium constants. The qualitative difference at high concentrations (divergence for Monte Carlo scheme and convergence for the coarse-grained model) arises from the significantly differing absolute values of the salt concentrations in the charge-inverted regime. This effect might be caused by several factors. First, the two schemes account for the multivalent ions in different ways and, thus, display different ionic strength and electrostatic screening. The Monte Carlo method takes into account the free  $YCl_3$ , monovalent counterions of the protein, and the additional monovalent NaCl ions and neglects monovalent  $Cl^-$  counterions to the bound yttrium ions. The coarse-grained model uses the full  $YCl_3$  concentration in the determination of the screening length. Second, the binding parameters are determined differently as described in the section Theoretical Modeling. Third, the Monte Carlo scheme accounts explicitly also for correlations between the bound ions, while the coarse-grained model treats all bound ions in a mean-field picture. Finally, pH effects and charge regulation varying with multivalent salt concentration are only accounted for in the coarse-grained model.

The general consistency of the observed trends despite the difference in the simulation schemes suggests that these trends are rather robust properties of a protein in a solution containing multivalent ions. On the basis of these charge curves, effects on the phase behavior are estimated in the following section.

**Dependence of Transition Concentrations  $c_Y^*$  and  $c_Y^{**}$  on Ionic Strength.** The results on the dependence of the transition concentrations  $c_Y^*$  and  $c_Y^{**}$  of HSA solutions on monovalent salt are summarized in Figure 5. From the experimental results, a clear increase of the two transition concentrations is observed with increasing monovalent salt concentration. This trend is observed for all protein concentrations probed in the range between 5 and 50 mg/mL (Figure 5a). For samples with  $c_{\text{NaCl}} \geq 100$  mM, no reentrant phase behavior is observed, and even samples at very high  $c_Y \geq 100$  mM are still turbid.

For the theoretical methods, the results differ between the estimation methods and simulation schemes. While  $c_Y^*$  from the charge estimation shows a clear increase for the full monovalent salt range (Figure 5b,c) (and thus agrees with the experimental observations (Figure 5a)),  $c_Y^*$  from the barrier estimation decreases for higher ionic strengths (Figure 5d,e). In contrast, for  $c_Y^{**}$  only the results from the barrier estimation show the observed general increase, while the charge estimation misses the trends at least for smaller protein concentrations.

**Discussion: Nature of the Protein Interactions Driving the Reentrant Phase Behavior.** From a comparison of the different results from experimental phase diagrams, SAXS, and simulations, a consistent picture of the underlying protein

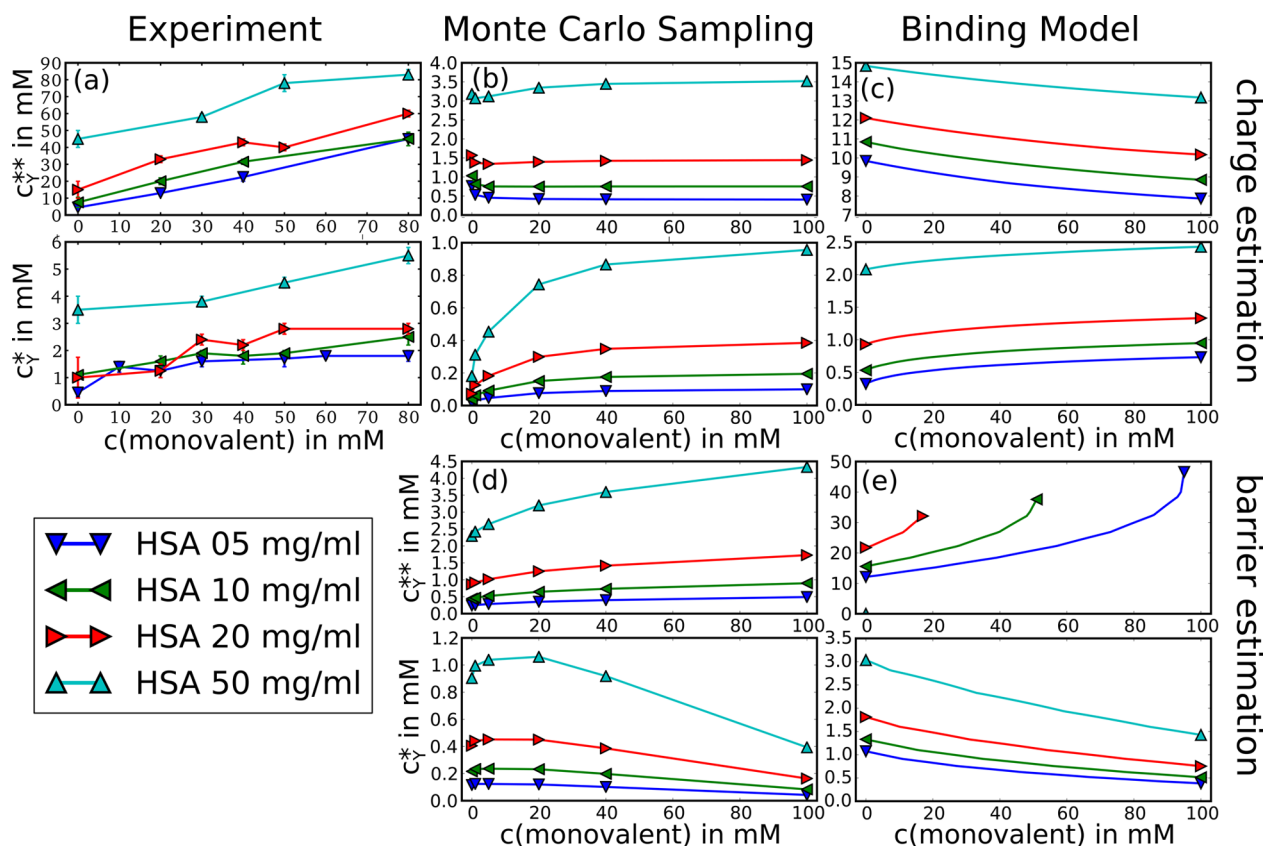


**Figure 5.** Transition concentrations  $c_Y^*$  and  $c_Y^{**}$  for the reentrant phase boundaries. The left column (a) summarizes the experimental results for the phase boundaries as determined by visual inspection at room temperature, showing a clear increase of both  $c_Y^*$  and  $c_Y^{**}$  with increasing monovalent salt. For  $c_{\text{NaCl}} \geq 100$  mM, no second transition is observed; the samples remain turbid up to very high  $c_Y \approx 100$  mM. The center and right columns show the results from the Monte Carlo sampling of binding configurations using the detailed protein structure (b, d) and the analytical coarse-grained model (c, e). Two estimations for  $c_Y^*$  and  $c_Y^{**}$  are used: The top row uses a critical charge of  $Q^* = -5e$  and  $Q^{**} = 5e$  as indicator (b, c). The bottom row estimates the transition concentration using the height of the repulsive barrier in the DLVO potential (d, e). For the analytical coarse-grained model (c, e), the curve corresponds to 100 data points that were not explicitly drawn for clarity. For the data points missing in (e) compared to (c), no repulsive barrier above  $1 k_B T$  was found. We remark that  $c_Y$  for the Monte Carlo method (b, d) has been estimated from the free ion concentration and the number of bound ions at a single protein molecule as described in the text.

interactions can be drawn for both the first transition  $c_Y^*$  and the second transition  $c_Y^{**}$ . The general picture involves charge-stabilized solutions at low and high  $c_Y$ , i.e., repulsive Coulomb interaction due to considerable protein net charges, while in the aggregation regime II an overall attractive interaction dominates. The competition of the attractive and repulsive interaction can be exploited by the addition of NaCl, thereby fine-tuning the interactions in both interaction strength and repulsion range. The occurring changes in protein interaction are schematically depicted in Figure 6 and will be discussed in the following for the two transitions. Starting from the experimental evidence by visual inspection and SAXS, the simulation results are used to provide insight into the underlying mechanisms of the ion–protein interaction.

A recent study investigated protein interactions in the presence of a set of mono-, di-, and trivalent counterions, indicating stronger changes of attraction and repulsion at similar ionic strength for multivalent ions compared to monovalent ions.<sup>50</sup> These findings clearly suggest an effect of multivalent ions beyond charge screening and are consistent with the interpretation for HSA and  $Y^{3+}$  concentrations below  $c_Y^*$ . While the present study focused on protein solutions with NaCl and  $YCl_3$ , comparable effects are also expected for other

multivalent ions as long as they also show considerable binding to protein functional groups.

In protein solutions with little or no  $YCl_3$ , the notion of a charge-stabilized solution is supported clearly by the SAXS results and the excellent agreement with model fits involving a screened Coulomb repulsion (Figure 3a). The correlation peak indicates the overall repulsion that becomes weaker once the ionic strength increases.

When the  $YCl_3$  concentration is increased, the first transition  $c_Y^*$  occurs. The experimental observation of  $c_Y^*$  for increasing NaCl concentration (Figure 5a) agrees well with the trend observed by SAXS (Figure 3c). With increasing  $c_{\text{NaCl}}$  the sample conditions move away from the phase boundary into the stable solution regime I (Figure 1), and the overall interaction has to become less attractive. Importantly, this trend cannot be caused by charge screening, since for net-negative proteins around  $c_Y^*$  charge screening would increase the overall attraction by a diminished repulsion for higher ionic strengths. By use of the simulation results, the mechanism behind the first transition can be elucidated. The increase of  $c_Y^*$  seems to be related rather to a critical charge  $Q^*$  (Figure 5b,c) than to a critical repulsive barrier (Figure 5d,e). While counterintuitive at first glance, this finding can be rationalized by a consideration of the nature of the attractive interaction throughout the phase

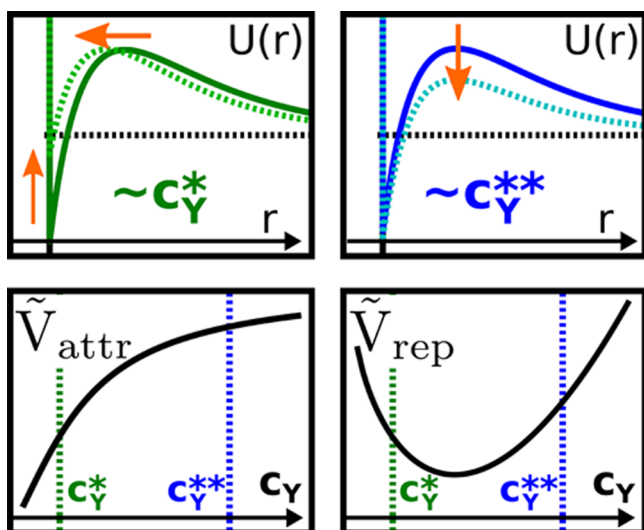


**Figure 6.** Schematic representation of the change of protein interaction throughout the phase diagram. The orange arrows indicate trends with increasing  $c_{\text{NaCl}}$ . Around  $c_Y^*$ , the addition of NaCl results in a weaker overall attraction, although the Coulomb repulsion is screened (top left). Around  $c_Y^{**}$ , the repulsion is screened with no evidence for varied attraction (top right). The addition of  $\text{YCl}_3$  has several simultaneous effects on the strength of attraction,  $\tilde{V}_{\text{attr}}$  (bottom left), and repulsion,  $\tilde{V}_{\text{rep}}$  (bottom right). First, the increase of the ionic strength shortens the repulsion range. Second, ion binding to the protein surface causes a charge inversion and, thus, changes the repulsion strength nonmonotonically (bottom right). Third, the presence of multivalent ions causes an additional attractive interaction, presumably mediated by ion bridges (bottom left).

diagram. Multivalent metal ions can form ion-mediated intermolecular salt bridges between globular proteins<sup>51</sup> and by these contribute considerably to the attraction. Ion-induced attraction is also suggested by a related experimental finding: HSA solutions without salt are stable even at the isoelectric point around pH 4.7.<sup>52</sup> Since the isoelectric point corresponds to zero net charge and vanishing Coulomb monopole repulsion, the attraction without salt is not strong enough to cause aggregation. Thus, the reentrant condensation in the presence of multivalent ions implies that the ions indeed play an essential role for the attractive interaction,<sup>27</sup> most likely via ion bridging.<sup>51,53</sup> A comparable mechanism might be present in the cross-linking of polymers or membranes.<sup>54,55</sup> Similar results on the competing salt effects on protein interactions have been found in simulations of calmodulin.<sup>56</sup> In this case, a decreased attraction with increasing monovalent salt concentration in the presence of trivalent cations is attributed to the ion–ion correlations of the bound multivalent cations.

Since the protein net charge is reflecting ion binding, the critical charge corresponds to a critical number of bound ions that allow enough ion-induced attraction to destabilize the protein solution and at the same time neutralize the protein net charge. By contrast, the barrier estimation uses a constant attraction represented by the Hamaker constant. The increase of  $c_Y^*$  with monovalent salt is thus most likely due to the effect of monovalent salt on the binding equilibrium of multivalent salts to the protein surface and interestingly not due to a stronger charge screening of Coulomb repulsion due to higher ionic strengths.

For the second transition ( $c_Y^{**}$ ), a different picture is found. The increasing trend of the experimental transition concen-

trations  $c_Y^{**}$  (Figure 5a) suggests stronger attraction and weaker repulsion with increasing  $c_{\text{NaCl}}$ , since the phase boundary from the reentrant regime III to the phase-separated regime II (Figure 1) is approached with increasing  $c_{\text{NaCl}}$ . This behavior agrees with the picture of a screened Coulomb repulsion. By use of the simulation results, the importance of Coulomb repulsion for the solution stability of the reentrant regime III is supported. The increase of  $c_Y^{**}$  for all protein concentrations is reproduced by the barrier estimation and not by the charge estimation (Figure 5b–e). This finding implies that charge is not enough to stabilize suspensions once the ionic strength is too high: Although the protein charge increases with monovalent salt concentration at fixed multivalent salt concentration, this gain in positive charge is not enough to overcome the effects of charge screening. Experimentally, this argument is further confirmed by the missing second transition  $c_Y^{**}$  for  $c_{\text{NaCl}} > 100$  mM and the strong increase of precipitating aggregates with increasing  $c_{\text{NaCl}}$  (cf. protein concentrations in the measured supernatant in Figure 3b). Considering the arguments on ion bridging from the previous paragraph on  $c_Y^*$ , a constant attraction, as used in the barrier estimation, is a reasonable assumption at high multivalent salt concentration: Once several ions have bound to the protein surface, further ions cannot contribute additional attraction via ion bridges for steric reasons. We therefore infer that charge screening plays the primary role for the reentrant transition  $c_Y^{**}$ , while ion binding is only a secondary effect.

The SAXS results around  $c_Y^{**}$  demonstrate that the underlying mechanism of the second transition is far from trivial. The increasing amount of precipitated aggregates with increasing  $c_{\text{NaCl}}$  (cf.  $c_{\text{HSA}}$  in the supernatant in Figure 3b) clearly indicates an overall increased attraction, consistent with the arguments of the previous paragraph. The low  $q$  behavior of the scattering intensity suggests the presence of larger aggregates in the supernatant measured after centrifugation (Figure 3b). From these results, aggregates seem to play an important role around  $c_Y^{**}$ . We emphasize that the formation of protein clusters in the presence of  $\text{YCl}_3$  has also been observed using dynamic and static light scattering in solutions of bovine serum albumin. While solutions with only NaCl could be described well with colloid theory based on monomers,<sup>39</sup> the addition of  $\text{YCl}_3$  induced signatures of cluster formation already for  $\text{Y}^{3+}$  concentrations below  $c_Y^*$ .<sup>58</sup>

At this point it is important to also note the limitations of the two simulation schemes. Both schemes are designed for the calculation of ion binding to individual protein molecules with negligible effect of protein interaction on the binding. Real protein solutions, however, might form clusters and aggregates<sup>57,58</sup> that affect both charge regulation and binding equilibria considerably. In particular in the reentrant and aggregated regime, corresponding to higher multivalent salt concentrations, the stability of the protein solutions might be determined by other properties beyond those of the individual molecule. Furthermore, both schemes are based on theoretical estimations and literature values and involve no fitting of experimental observables. In particular, the large deviations in the absolute values for the transition concentrations between the Monte Carlo scheme and the experiments might be caused by a nonoptimized choice for the binding constant.

Despite these limitations, the comparison of both schemes helps to prevent conclusions from potential artifacts. The results of both simplified schemes reproduce the experimental observations semiquantitatively and lead to a consistent

interpretation with an attractive interaction caused by ion bridges and repulsion due to Coulomb interaction.

It is worth noting that both the reentrant phase behavior and the mechanism of ion condensation differ considerably from the reentrant condensation in DNA systems.<sup>19,23,24</sup> In the case of DNA, the ions condense because of ion–ion correlations, while the counterion–protein interaction is dominated by the binding of multivalent cations to carboxylic surface groups. The trend with increasing monovalent salt concentration for the second transition is opposite between the two systems. For proteins, the transition concentration  $c_{\text{Y}}^{**}$  increases, while it stays constant or decays in the case of DNA.<sup>23</sup>

## CONCLUSION

We have presented a comprehensive study of the impact of monovalent ions (NaCl) on the reentrant phase behavior of the globular protein HSA induced by  $\text{YCl}_3$ . Experimental data on the phase diagram and from small-angle X-ray scattering on the protein interaction have been compared to results from two simulation methods (a Monte Carlo sampling of binding configurations and an analytical coarse-grained model) on the protein net charges and the related solution stability. All results support a consistent picture of the protein interactions causing the reentrant phase diagram, as summarized schematically in Figure 6. By use of the effect of NaCl, effects of charge screening, i.e., diminishing Coulomb repulsion, could be separated from effects of increased attraction, providing insight into the nature of the underlying protein interaction.

At low  $\text{YCl}_3$  concentrations  $c_{\text{Y}}$ , screened Coulomb interaction is dominant. Approaching the first transition concentration  $c_{\text{Y}}^*$ , the binding of multivalent counterions not only reduces the net protein charge and Coulomb repulsion but importantly also contributes to the attractive interaction between the proteins, probably by ion bridging between molecules<sup>51,53</sup> or ion–ion correlations of bound cations.<sup>56</sup> Under these conditions, a higher ionic strength, although screening the Coulomb repulsion, decreases the overall attraction, since less counterions bind to the surface (Figure 4). As observed in the experiments, the transition concentration  $c_{\text{Y}}^*$  increases with increasing  $c_{\text{NaCl}}$ . The finding that the first transition is driven by the ion-induced increase of attraction (Figure 6) is supported by the SAXS results (Figure 3c) and the transition concentrations based on the charge estimation (Figure 5).

For  $c_{\text{Y}}^{**}$ , a different mechanism appears to be dominant. An increasing ionic strength decreases the Coulomb repulsion and renders charge stabilization of the protein solution only possible for higher protein charges, i.e., more bound counterions. Although more multivalent counterions are bound for higher  $c_{\text{NaCl}}$  (Figure 4), the effect of charge screening overcompensates the gain in charge, as seen from the barrier estimation in Figure 5. Consistent with the experiments,  $c_{\text{Y}}^{**}$  thus increases with increasing  $c_{\text{NaCl}}$ . These results support that the change of the second transition with increasing  $c_{\text{NaCl}}$  is driven by the reduction of repulsion due to charge screening (Figure 6). The related SAXS results suggest a relevant role of aggregates around the second transition.

In summary, the present study provides a consistent picture of the underlying interactions driving the reentrant condensation in protein solutions in the presence of  $\text{YCl}_3$ . Monovalent salt tunes the interaction strength and the range of interaction. The competition of binding of multivalent ions and nonspecific effects of monovalent salts provides interesting opportunities to tune interactions in solutions.

## AUTHOR INFORMATION

### Corresponding Authors

\*F.R.-R.: e-mail, roosen-runge@ill.eu.

\*F.Z.: e-mail, fajun.zhang@uni-tuebingen.de.

### Author Contributions

#E.J. and F.R.-R. contributed equally to this paper.

### Notes

The authors declare no competing financial interest.

## ACKNOWLEDGMENTS

We are grateful for the valuable discussions and comments from T. Narayanan (ESRF, Grenoble, France). We gratefully acknowledge financial support from the Deutsche Forschungsgemeinschaft (DFG). F.R.-R. acknowledges a fellowship of the Studienstiftung des Deutschen Volkes. E.J. acknowledges a studentship of the Institut Laue-Langevin (Grenoble, France).

## REFERENCES

- (1) Hofmeister, F. Zur Lehre von der Wirkung der Salze. *Naunyn-Schmiedeberg's Arch. Pharmacol.* **1888**, *24*, 247–260.
- (2) Collins, K. D. Ions from the Hofmeister Series and Osmolytes: Effects on Proteins in Solution and in the Crystallization Process. *Methods* **2004**, *34*, 300–311.
- (3) Curtis, R. A.; Prausnitz, J. M.; Blanch, H. W. Protein–Protein and Protein–Salt Interactions in Aqueous Protein Solutions Containing Concentrated Electrolytes. *Biotechnol. Bioeng.* **1998**, *57*, 11–21.
- (4) Das, R.; Mills, T. T.; Kwok, L. W.; Maskel, G. S.; Millett, I. S.; Doniach, S.; Finkelstein, K. D.; Herschlag, D.; Pollack, L. Counterion Distribution around DNA Probed by Solution X-ray Scattering. *Phys. Rev. Lett.* **2003**, *90*, 188103.
- (5) Manning, G. S. The Molecular Theory of Polyelectrolyte Solutions with Applications to the Electrostatic Properties of Polynucleotides. *Q. Rev. Biophys.* **1978**, *11*, 179–246.
- (6) Deserno, M.; Holm, C.; May, S. Fraction of Condensed Counterions around a Charged Rod: Comparison of Poisson–Boltzmann Theory and Computer Simulations. *Macromolecules* **2000**, *33*, 199–206.
- (7) Moreira, A. G.; Netz, R. R. Strong-Coupling Theory for Counterion Distributions. *Europhys. Lett.* **2000**, *52*, 705.
- (8) Grosberg, A. Y.; Nguyen, T. T.; Shklovskii, B. I. Colloquium: The Physics of Charge Inversion in Chemical and Biological Systems. *Rev. Mod. Phys.* **2002**, *74*, 329–345.
- (9) Besteman, K.; Zevenbergen, M. A. G.; Heering, H. A.; Lemay, S. G. Direct Observation of Charge Inversion by Multivalent Ions as a Universal Electrostatic Phenomenon. *Phys. Rev. Lett.* **2004**, *93*, 170802.
- (10) Messina, R. Electrostatics in Soft Matter. *J. Phys.: Condens. Matter* **2009**, *21*, 113102.
- (11) Lyklema, J. Overcharging, Charge Reversal: Chemistry or Physics? *Colloids Surf., A* **2006**, *291*, 3–12.
- (12) Jungwirth, P.; Winter, B. Ions at Aqueous Interfaces: From Water Surface to Hydrated Proteins. *Annu. Rev. Phys. Chem.* **2008**, *59*, 343–366.
- (13) Lund, M.; Vrbka, L.; Jungwirth, P. Specific Ion Binding to Nonpolar Surface Patches of Proteins. *J. Am. Chem. Soc.* **2008**, *130*, 11582–11583.
- (14) Kalcher, I.; Horinek, D.; Netz, R. R.; Dzubiella, J. Ion Specific Correlations in Bulk and at Biointerfaces. *J. Phys.: Condens. Matter* **2009**, *21*, 424108.
- (15) Kubíčková, A.; Křížek, T.; Coufal, P.; Vazdar, M.; Wernersson, E.; Heyda, J.; Jungwirth, P. Overcharging in Biological Systems: Reversal of Electrophoretic Mobility of Aqueous Polyaspartate by Multivalent Cations. *Phys. Rev. Lett.* **2012**, *108*, 186101.
- (16) Harding, M. M. Geometry of Metal–Ligand Interactions in Proteins. *Acta Crystallogr., Sect. D* **2001**, *57*, 401–411.
- (17) Permyakov, E. Y. *Metalloproteomics*; John Wiley & Sons: Hoboken, NJ, 2009.

- (18) Andresen, K.; Das, R.; Park, H. Y.; Smith, H.; Kwok, L. W.; Lamb, J. S.; Kirkland, E. J.; Herschlag, D.; Finkelstein, K. D.; Pollack, L. Spatial Distribution of Competing Ions around DNA in Solution. *Phys. Rev. Lett.* **2004**, *93*, 248103.
- (19) Burak, Y.; Ariel, G.; Andelman, D. Competition between Condensation of Monovalent and Multivalent Ions in DNA Aggregation. *Curr. Opin. Colloid Interface Sci.* **2004**, *9*, 53–58.
- (20) Nguyen, T. T.; Grosberg, A. Y.; Shklovskii, B. I. Macroions in Salty Water with Multivalent Ions: Giant Inversion of Charge. *Phys. Rev. Lett.* **2000**, *85*, 1568–1571.
- (21) Lenz, O.; Holm, C. Simulation of Charge Reversal in Salty Environments: Giant Overcharging? *Eur. Phys. J. E* **2008**, *26*, 191–195.
- (22) Sandhu, R. S. A Thermodynamic Study of Complexation Reaction of Yttrium(III), Lanthanum(III) and Cerium(III) with Tyrosine. *Monatsh. Chem.* **1977**, *108*, 51–55.
- (23) Saminathan, M.; Antony, T.; Shirahata, A.; Sigal, L. H.; Thomas, T.; Thomas, T. J. Ionic and Structural Specificity Effects of Natural and Synthetic Polyamines on the Aggregation and Resolubilization of Single-, Double-, and Triple-Stranded DNA. *Biochemistry* **1999**, *38*, 3821–3830.
- (24) Nguyen, T. T.; Rouzina, I.; Shklovskii, B. I. Reentrant Condensation of DNA Induced by Multivalent Counterions. *J. Chem. Phys.* **2000**, *112*, 2562–2568.
- (25) Zhang, F.; Skoda, M. W. A.; Jacobs, R. M. J.; Zorn, S.; Martin, R. A.; Martin, C. M.; Clark, G. F.; Weggler, S.; Hildebrandt, A.; Kohlbacher, O.; Schreiber, F. Reentrant Condensation of Proteins in Solution Induced by Multivalent Counterions. *Phys. Rev. Lett.* **2008**, *101*, 148101.
- (26) Zhang, F.; Weggler, S.; Ziller, M. J.; Ianeselli, L.; Heck, B. S.; Hildebrandt, A.; Kohlbacher, O.; Skoda, M. W. A.; Jacobs, R. M. J.; Schreiber, F. Universality of Protein Reentrant Condensation in Solution Induced by Multivalent Metal Ions. *Proteins* **2010**, *78*, 3450–3457.
- (27) Roosen-Runge, F.; Heck, B. S.; Zhang, F.; Kohlbacher, O.; Schreiber, F. Interplay of pH and Binding of Multivalent Metal Ions: Charge Inversion and Reentrant Condensation in Protein Solutions. *J. Phys. Chem. B* **2013**, *117*, 5777–5787.
- (28) Narayanan, T. Synchrotron Small-Angle X-ray Scattering. In *Soft Matter Characterization*; Borsali, R., Pecora, R., Eds.; Springer: New York, 2008; p 899 ff.
- (29) Glatter, O.; Kratky, O. *Small Angle X-ray Scattering*; Academic Press: New York, 1982; p 515.
- (30) Svergun, D. I.; Koch, M. H. J. Small-Angle Scattering Studies of Biological Macromolecules in Solution. *Rep. Prog. Phys.* **2003**, *66*, 1735.
- (31) Hansen, J.-P.; McDonald, I. R. *Theory of Simple Liquids*, 3rd ed.; Elsevier: Amsterdam, 2006.
- (32) Pedersen, J. S. Analysis of Small-Angle Scattering Data from Colloids and Polymer Solutions: Modeling and Least-Squares Fitting. *Adv. Colloid Interface Sci.* **1997**, *70*, 171–210.
- (33) Chen, S. H.; Lin, T. L. In *Neutron Scattering*; Price, D. L., Sködl, K., Eds.; Academic Press: London, 1987; pp 489–543.
- (34) Zhang, F.; Skoda, M. W. A.; Jacobs, R. M. J.; Martin, R. A.; Martin, C. M.; Schreiber, F. Protein Interactions Studied by SAXS: Effect of Ionic Strength and Protein Concentration for BSA in Aqueous Solutions. *J. Phys. Chem. B* **2007**, *111*, 251–259.
- (35) Feigin, L. A.; Svergun, D. I. *Structure Analysis by Small-Angle X-Ray and Neutron Scattering*; Plenum Press: New York, 1987.
- (36) Ishihara, A. Determination of Molecular Shape by Osmotic Measurement. *J. Chem. Phys.* **1950**, *18*, 1446–1449.
- (37) Zhang, F.; Roosen-Runge, F.; Skoda, M. W. A.; Jacobs, R. M. J.; Wolf, M.; Callow, P.; Frielinghaus, H.; Pipich, V.; Prevost, S.; Schreiber, F. Hydration and Interactions in Protein Solutions Containing Concentrated Electrolytes Studied by Small-Angle Scattering. *Phys. Chem. Chem. Phys.* **2012**, *14*, 2483–2493.
- (38) Nägele, G. On the Dynamics and Structure of Charge-Stabilized Suspensions. *Phys. Rep.* **1996**, *272*, 215–372.
- (39) Heinen, M.; Zanini, F.; Roosen-Runge, F.; Fedunova, D.; Zhang, F.; Hennig, M.; Seydel, T.; Schweins, R.; Sztucki, M.; Antalik, M.; Schreiber, F.; Nägele, G. Viscosity and Diffusion: Crowding and Salt Effects in Protein Solutions. *Soft Matter* **2012**, *8*, 1404–1419.
- (40) Hayter, J. B.; Penfold, J. An Analytic Structure Factor for Macroion Solutions. *Mol. Phys.* **1981**, *42*, 109–118.
- (41) Hansen, J.-P.; Hayter, J. B. A Rescaled MSA Structure Factor for Dilute Charged Colloidal Dispersions. *Mol. Phys.* **1982**, *46*, 651–656.
- (42) Kline, S. R. Reduction and Analysis of SANS and USANS Data Using IGOR Pro. *J. Appl. Crystallogr.* **2006**, *39*, 895–900.
- (43) Wardell, M.; Wang, Z.; Ho, J. X.; Robert, J.; Ruker, F.; Ruble, J.; Carter, D. C. The Atomic Structure of Human Methemalbumin at 1.9 Å. *Biochem. Biophys. Res. Commun.* **2002**, *291*, 813–819.
- (44) Bashford, D.; Karplus, M. pKa's of Ionizable Groups in Proteins: Atomic Detail from a Continuum Electrostatic Model. *Biochemistry* **1990**, *29*, 10219–10225.
- (45) Gordon, J. C.; Myers, J. B.; Folta, T.; Shoja, V.; Heath, L. S.; Onufriev, A. H++. A Server for Estimating pKas and Adding Missing Hydrogens to Macromolecules. *Nucleic Acids Res.* **2005**, *33*, W368–W371.
- (46) Likos, C. N. Effective Interactions in Soft Condensed Matter Physics. *Phys. Rep.* **2001**, *348*, 267–439.
- (47) Roosen-Runge, F.; Hennig, M.; Seydel, T.; Zhang, F.; Skoda, M. W.; Zorn, S.; Jacobs, R. M.; Maccarini, M.; Fouquet, P.; Schreiber, F. Protein Diffusion in Crowded Electrolyte Solutions. *Biochim. Biophys. Acta, Proteins Proteomics* **2010**, *1804*, 68–75.
- (48) Zhang, F.; Roth, R.; Wolf, M.; Roosen-Runge, F.; Skoda, M. W. A.; Jacobs, R. M. J.; Sztucki, M.; Schreiber, F. Charge-Controlled Metastable Liquid–Liquid Phase Separation in Protein Solutions as a Universal Pathway towards Crystallization. *Soft Matter* **2012**, *8*, 1313–1316.
- (49) Fukasawa, T.; Sato, T. Versatile Application of Indirect Fourier Transformation to Structure Factor Analysis: From X-ray Diffraction of Molecular Liquids to Small Angle Scattering of Protein Solutions. *Phys. Chem. Chem. Phys.* **2011**, *13*, 3187–3196.
- (50) Kundu, S.; Das, K.; Aswal, V. Modification of Attractive and Repulsive Interactions Among Proteins in Solution Due to the Presence of Mono-, Di- and Tri-Valent Ions. *Chem. Phys. Lett.* **2013**, *578*, 115–119.
- (51) Zhang, F.; Zocher, G.; Sauter, A.; Stehle, T.; Schreiber, F. Novel Approach to Controlled Protein Crystallization through Ligandation of Yttrium Cations. *J. Appl. Crystallogr.* **2011**, *44*, 755–762.
- (52) Dockal, M.; Carter, D. C.; Rükner, F. Conformational Transitions of the Three Recombinant Domains of Human Serum Albumin Depending on pH. *J. Biol. Chem.* **2000**, *275*, 3042–3050.
- (53) Roosen-Runge, F.; Zhang, F.; Schreiber, F.; Roth, R. Ion-Activated Attractive Patches as a Mechanism for Controlled Protein Interactions. Submitted 2014.
- (54) Rozycki, B.; Lipowsky, R.; Weikl, T. R. Effective Surface Interactions Mediated by Adhesive Particles. *Europhys. Lett.* **2008**, *84*, 26004.
- (55) Heyda, J.; Muzdalo, A.; Dzubiella, J. Rationalizing Polymer Swelling and Collapse under Attractive Cosolvent Conditions. *Macromolecules* **2013**, *46*, 1231–1238.
- (56) Lund, M.; Jönsson, B. A Mesoscopic Model for Protein–Protein Interactions in Solution. *Biophys. J.* **2003**, *85*, 2940–2947.
- (57) Stradner, A.; Sedgwick, H.; Cardinaux, F.; Poon, W. C. K.; Egelhaaf, S. U.; Schurtenberger, P. Equilibrium Cluster Formation in Concentrated Protein Solutions and Colloids. *Nature* **2004**, *432*, 492–495.
- (58) Soraruf, D.; Roosen-Runge, F.; Grimaldo, M.; Zanini, F.; Schweins, R.; Seydel, T.; Zhang, F.; Roth, R.; Oettel, M.; Schreiber, F. Protein Cluster Formation in Aqueous Solution in the Presence of Multivalent Metal Ions—A Light Scattering Study. *Soft Matter* **2014**, *10*, 894–902.